J Mater Sci (2011) 46:3073–3083
DOI 10.1007/s10853-010-5186-9

Kinetics of fly ash geopolymerization

Chen Chen · Weiliang Gong · Werner Lutze · Ian L. Pegg

Received: 22 July 2010 / Accepted: 10 December 2010 / Published online: 29 December 2010
© Springer Science+Business Media, LLC 2010

Abstract Based on the wet chemical analysis, we measured and modeled the kinetics of reactions between fly ash and KOH at various temperatures and water-to-solid mass ratios (*W/S*). We find that three consecutive rate-limiting processes control reaction progress: (1) dissolution or alteration of the glass phase in the fly ash, (2) classical Fick diffusion through a surface layer, and (3) diffusive transport through a more complex gel structure (interstitial gel). This sequence of processes is independent of *W/S* (0.35–40), temperature (22–75 °C), and KOH concentration (5–10 M). The relative contribution of each process to the overall reaction progress changes with experimental conditions. Only if and when the third process is rate limiting, a fly ash geopolymer forms and develops mechanical strength (sufficiently low *W/S* ratio provided). The rate of reaction progress decreases significantly, due to slow transport of reacting species to the surface of the glass particles.

Introduction

In a previous article, Chen et al. [1] describe a procedure to evaluate the reactivity of fly ashes in alkaline solutions as a function of pH and temperature. This procedure allowed us to study the kinetics of fly ash dissolution, gel formation, and related processes over a range of water-to-solid mass ratios (*W/S*), including those typical of geopolymer pastes. A summary of literature related to fly ash reactivity can be found in the previous article [1]. In the present article, we show that the process of corrosion of the glass in fly ash remains the same when the water-to-solid ratio is lowered to that typical of geopolymer pastes. The techniques to study the process become more challenging at low *W/S*. The progress of leaching and the important relationship between reaction kinetics and gain of compressive strength are discussed.

C. Chen · W. Gong (✉) · W. Lutze · I. L. Pegg
Vitreous State Laboratory, The Catholic University of America, Washington, DC, USA
e-mail: gongw@vsl.cua.edu

C. Chen
State Key Laboratory of Pollution Control and Resources Reuse and School of the Environment, Nanjing University, Nanjing 210093, People's Republic of China

Materials and methods

Class F Headwater (HW) fly ash from Orlando, Florida was used in this study. The fly ash contains 77 wt% glass, 13.4 wt% mullite, quartz, magnetite, and 9.6 wt% unburned carbon. About 80% of the glass particles are larger than 10 μm and smaller than 100 μm. The composition of the fly ash is given in [1].

We synthesized the glass phase of the fly ash to conduct X-ray diffraction studies without interference from the accompanying crystalline phases. The synthetic glass contained 8 wt% instead of 4 wt% Na_2O to lower the melting temperature to about 1,500 °C. We reacted the crushed glass with 7.5 M KOH at 75 °C following procedures described below for the fly ash. The findings are part of the "Discussion" section.

The HW fly ash was leached up to 28 days in KOH solutions (5, 7.5, and 10 M) at 22, 35, 50, and 75 °C. One part of the leaching experiments was conducted using water-to-fly ash mass ratios (*W/S*) of 40, 10, 5, and 1, high enough for setting of the slurry not to occur. In another part, *W/S* was 0.35 to allow for setting and hardening. After

leaching at the higher *W/S* ratios, the slurry was filtered. The particles were washed with deionized water, suspended in absolute alcohol to terminate hydration, and dried at 105 °C. The particles were treated with dilute HCl to dissolve reaction products [1] and the mass loss was determined. Leachates were analyzed quantitatively by direct current plasma atomic emission spectrometry (DCP-AES).

At $W/S = 0.35$, a paste formed upon mixing of fly ash and KOH solution. Samples were cured at various temperatures but the setting time was not measured. The *W/S* ratio of 0.35 yields a paste, which is workable for several hours before it sets and hardens. Experiments were conducted as follows: after mixing KOH solution with fly ash, the paste was filled into cylindrical molds, one inch wide and three inches long. The containers were sealed with a lid and demoulded at the end of the curing period. At 50 and 75 °C, curing periods were up to 28 days, and at 20 and 35 °C, up to 300 days. Compressive strength was measured on 1 × 3-inch-samples with an Instron Model 5566 instrument. The cured samples were crushed and ground and 5 g of the powder was suspended in absolute ethanol, filtered and dried at 105 °C, then washed with water to remove remaining unreacted KOH, then filtered and dried again. Dried material was leached in dilute HCl to dissolve reaction products [1] and then the mass loss was determined. Samples from all experiments were characterized by X-ray diffraction (XRD) and scanning electron microscopy/energy dispersive X-ray spectrometry (SEM/EDS). Herein, we define the reactivity of fly ash by (1):

$$\frac{\mathrm{d}\alpha}{\mathrm{d}t} = \frac{1}{m_0} \cdot \frac{\mathrm{d}m_t}{\mathrm{d}t} \tag{1}$$

and reaction progress by

$$\alpha_t = \frac{\Delta m(t)}{m_0} = \frac{m_0 - m_t}{m_0} \tag{2}$$

where, m_o is the initial mass of fly ash and m_t is the residual mass at time t after leaching in alkali hydroxide and subsequent dissolution of reaction products with diluted HCl. In this work, we use increments of mass loss and characterize reactivity in terms of reaction progress. We apply reaction progress to fly ash in its entirety, not only to the glass phase. Therefore, reaction progress does not reach 100% in the presence of constituents much less reactive than the glass. For HW fly ash, α_{max} is approximately 0.77. The apparent relative mass loss α_t' is

$$\alpha_t' = \frac{m_0 - m_t'}{m_0} \tag{3}$$

where m_t' is the residual mass after leaching in alkaline solution. α_t' measures the mass of glass actually dissolved only as long as the mass of glass converted into gel is negligible. The relative mass of solid reaction products, β_t', is

$$\beta_t' = \frac{m_t' - m_t}{m_0} \tag{4}$$

Results

Figure 1 shows the effect of the water-to-solid ratio (*W/S*) on reaction progress during leaching of HW fly ash in 7.5 M KOH at 75 °C. At all *W/S* ratios reaction progress increases with time, the rate decreases. At higher *W/S* ratios (5, 10, and 40), reaction progress reaches 0.70 after 340 h, i.e., 90% consumption of the glass. At lower *W/S* ratios (0.35, 1.0), reaction progress is lower. In the beginning, reactivity appears to depend little on *W/S*; the solution is free of glass constituents and the glass surface is not yet covered with gel, allowing the glass to dissolve at its highest possible rate at a given temperature [1].

Figure 2a shows the effect of *W/S* on the relative mass of gel (Eq. 4) formed from glass in HW fly ash as a function of reaction progress (7.5 M KOH, 75 °C). Figure 2b complements Fig. 2a, by showing the fraction of glass apparently dissolved (Eq. 3). At $W/S = 40$ (Fig. 2a), significant gel formation begins at $\alpha_t \approx 0.4$, in all other cases at $\alpha_t < 0.2$. Correspondingly, Fig. 2b ($W/S = 40$) shows considerable glass dissolution at $\alpha_t < 0.4$, and much less at lower *W/S* ratios. Decreasing values of α_t' in Fig. 2b mean that the sample gained weight upon further leaching. There are no data for $W/S = 0.35$ because the small amount of liquid could not be separated from the solid.

Concerning the slopes $\Delta\beta_t'/\Delta\alpha_t$ in Fig. 2a, we distinguish four cases: if $\Delta\beta_t'/\Delta\alpha_t = 0$, glass simply dissolves, if

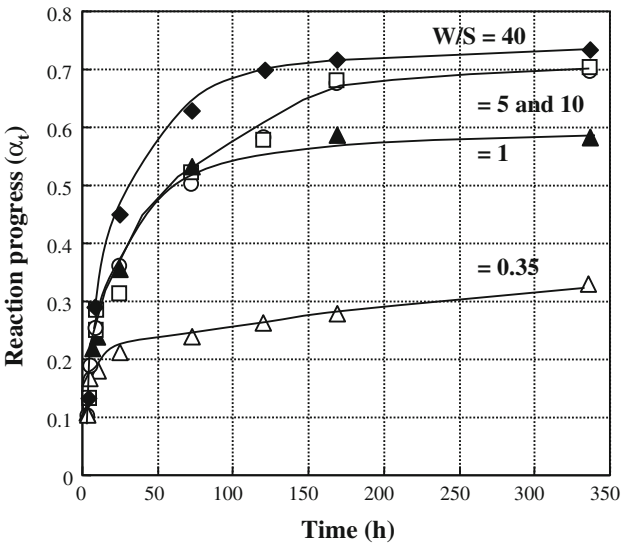

Fig. 1 Effect of water-to-solid ratio on reaction progress (7.5 M KOH, 75 °C)

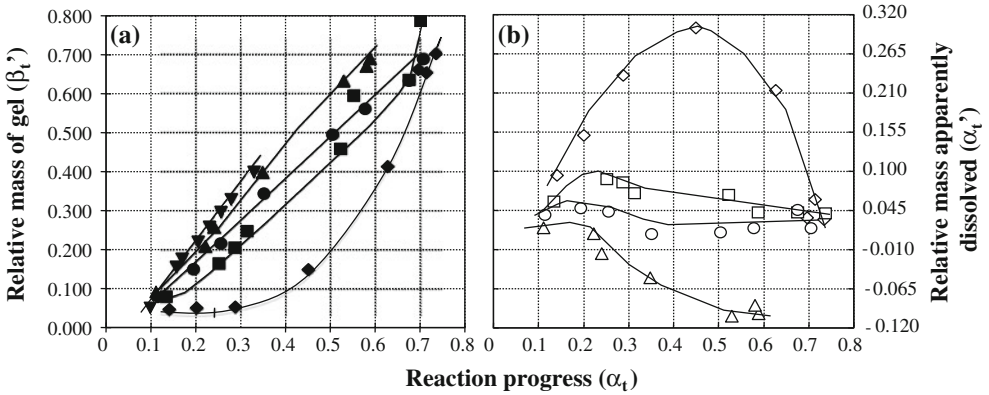

Fig. 2 Effect of water-to-solid ratio on gel formed and fly ash dissolved as a function of reaction progress (7.5 M KOH, 75 °C). **a** *filled diamond* 40, *filled square* 10, *filled circle* 5, *filled triangle* 1, *filled inverted triangle* 0.35, **b** *open diamond* 40, *open square* 10, *open circle* 5, *open triangle* 1

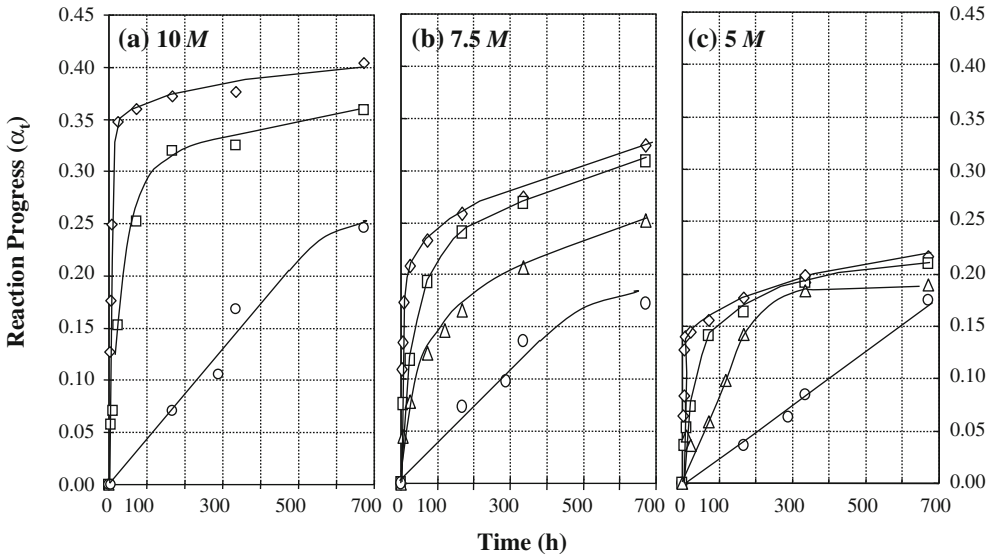

Fig. 3 Effect of temperature and KOH molarity on reaction progress during geopolymerization ($W/S = 0.35$). *Open circle* 22 °C, *open triangle* 35 °C, *open square* 50 °C, *open diamond* 75 °C

$\Delta\beta_t'/\Delta\alpha_t < 1$, the products of leaching are gel and dissolved glass; if $\Delta\beta_t'/\Delta\alpha_t \approx 1$, leaching yields practically only gel; if $\Delta\beta_t'/\Delta\alpha_t > 1$ glass corrosion yields gel and solution constituents participate significantly in surface layer formation. Figure 2a shows that, in the beginning, $0 < \Delta\beta_t'/\Delta\alpha_t < 1$ applies to all *W/S* ratios: none of the straight lines (extrapolated) intersects α_t at zero, i.e., in the beginning glass dissolves and little amount of gel forms [1]. At $W/S = 40$, $\Delta\beta_t'/\Delta\alpha_t$ is close to zero for $\alpha_t < 0.35$; at higher α_t values, the slope approaches $\Delta\beta_t'/\Delta\alpha_t \approx 2$. Here, gel formation was accompanied by massive precipitation of a zeolite ("Discussion" section). At $W/S = 5$, the slope $\Delta\beta_t'/\Delta\alpha_t \approx 1.1$ only a small amount of zeolite was detected. The curve for $W/S = 10$ reflects the transition between 40 and 5. At the *W/S* ratios of 1 and 0.35, the slope is greater than one but no new crystalline phase was detected by X-ray diffraction. However, potassium was found in the gel (Fig. 5).

Experiments underlying the results shown in Fig. 3 were conducted solely at $W/S = 0.35$, i.e., we are looking at the effects of KOH molarity and temperature on α_t in solidifying geopolymer pastes. In 10 M KOH (Fig. 3a), a reaction progress of 0.4 was reached at 75 °C and of about 0.20 at 22 °C after 672 h (28 days). Some pore water appears to be still present for α_t to increase at a low rate beyond 28 days. At lower KOH molarity (Fig. 3b, c), reaction progress is smaller but its temperature dependence remains qualitatively the same.

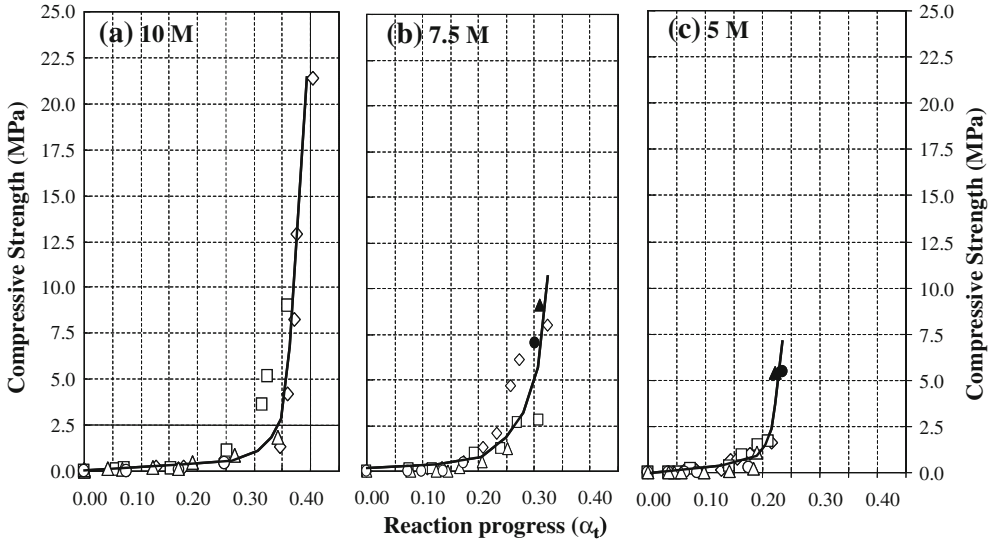

Fig. 4 Buildup of compressive strength during geopolymerization. *Open diamond* 75°C, *open square* 50 °C, *open triangle* 35 °C, *open circle* 22 °C, *filled symbols* for 22 or 35 °C, 300 days

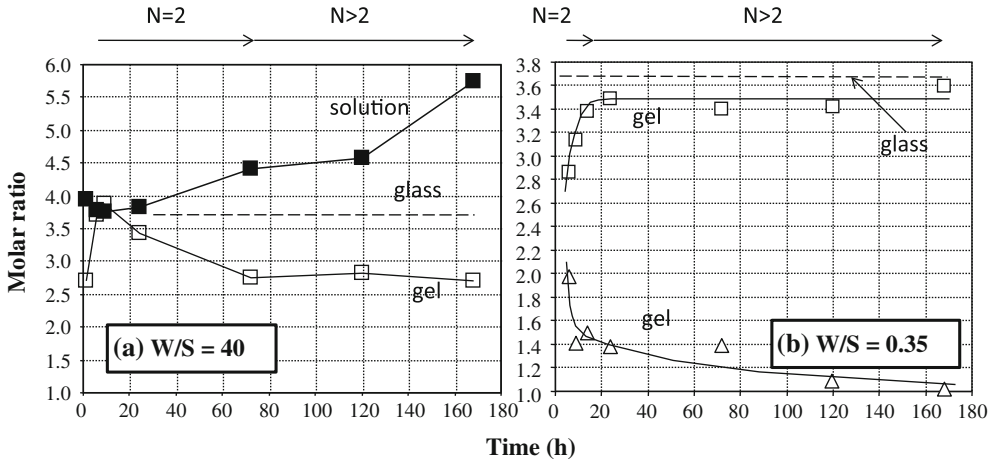

Fig. 5 Molar ratios of SiO_2/Al_2O_3 and K_2O/Al_2O_3 in interstitial gel (**a** 7.5 M; **b** 10 M KOH; 75 °C). *Filled square* and *open square* SiO_2/Al_2O_3, *open triangle* K_2O/Al_2O_3

Figure 4a–c shows the gain of compressive strength of geopolymer pastes as a function of reaction progress using all data from Fig. 3a–c, respectively. The pastes set and a compressive strength of about 1 MPa (145 psi) was attained at that point. A comparison of plots A, B, and C in Fig. 4 shows that setting begins between $\alpha_t = 0.15$ (5 M KOH) and $\alpha_t = 0.25$ (10 M KOH). Increasing the KOH molarity caused a stronger increase of strength than increasing the temperature. A rise in temperature from 22 to 75 °C with 10 M KOH (Fig. 4) accelerated the gain in compressive strength such that the sample cured at 75 °C had 20 times higher compressive strength (22 MPa) after 672 h ($\alpha_t = 0.41$) than that cured at 22 °C ($\approx$1 MPa) after the same time ($\alpha_t = 0.15$). Filled symbols (22 and 35 °C) in Fig. 4 are data from 300 day experiments.

Figure 5a shows SiO_2/Al_2O_3 ratios as they change over time, i.e., with reaction progress, in the gel phase and in solution at $W/S = 40$. Figure 5b shows the SiO_2/Al_2O_3 ratio and the K_2O/Al_2O_3 ratio in the gel as they change at $W/S = 0.35$. This is discussed in "Discussion" section. The data shown in Fig. 5b were obtained by DCP/AES analysis of dissolved gel. SEM/EDS analyses of the solid samples were in fair agreement with DCP/AES data.

Figures 6, 7, and 8 show the formation of gel on and between fly ash glass particles as a function of time ($W/S = 0.35$). After 24 h in 10 M KOH at 75 °C, Fig. 6, gel is visible on and between glass particles. Spaces between particles are visible. We assume that the pore solution is supersaturated with dissolved silicon and aluminum species, which form the interstitial gel. This assumption is in

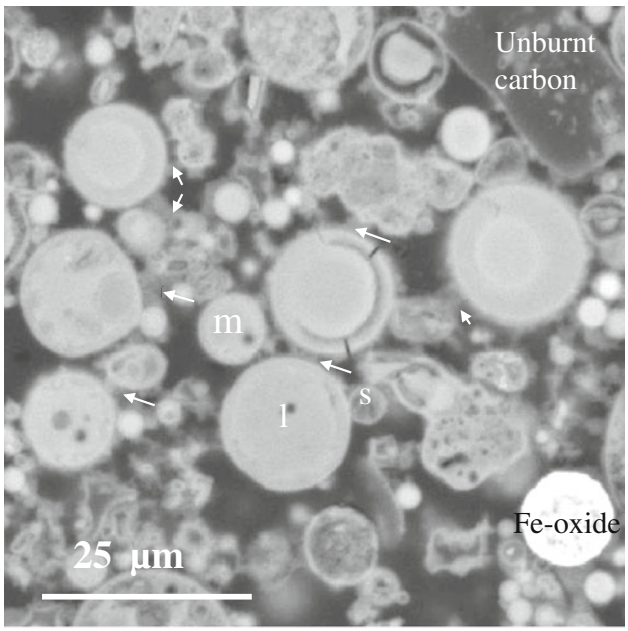

Fig. 6 SEM micrograph of Headwater fly ash after 24 h in 10 M KOH at 75 °C ($W/S = 0.35$); *l*, *m*, *s* large, medium, small, particle, respectively

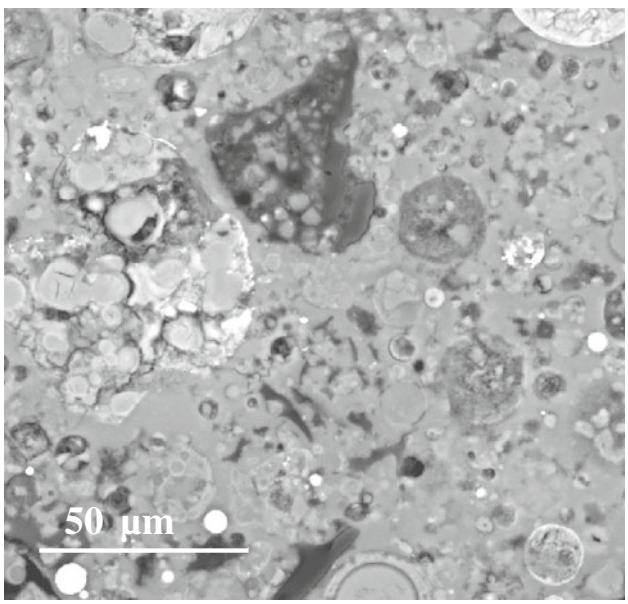

Fig. 7 SEM micrograph of Headwater fly ash after 28 days in 10 M KOH at 75 °C ($W/S = 0.35$)

agreement with the reaction sequence of geopolymerization proposed by Provis et al. [2] and Provis and van Deventer [3].

After 28 days, a continuous matrix phase, the light gray area, as shown in Fig. 7 has formed. Many glass particles are still visible within the gel matrix. Remaining glass

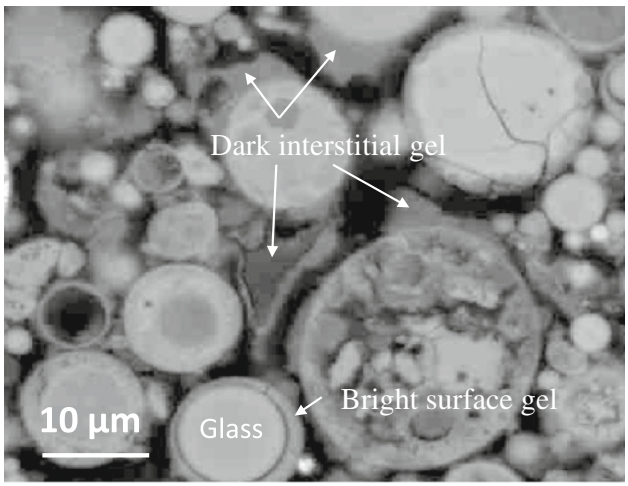

Fig. 8 Backscattered electron image of Headwater fly ash after 72 h in 7.5 M KOH at 75 °C ($W/S = 0.35$)

particles (e.g. on the bottom of Fig. 7) are surrounded by a reaction layer, lighter in color than the matrix phase gel. The matrix phase has hardened and is a practically water-free alkali aluminosilicate gel. Our finding that the weight loss in air of a $2'' \times 4''$ geopolymer cylinder corresponded very closely to the weight of the water used to make the cylinder supports this statement. Dissolving the gel shown in Fig. 7 in acid allowed us to determine the overall reaction progress. Figure 8 shows the two types of gel at an intermediate state of reaction. In this case, the fly ash was leached for 72 h in 7.5 M KOH at 75 °C. There is a lighter gel attached to the spherical glass particles and a darker gel filling the interstices.

Discussion

We have conducted leaching experiments with Headwater fly ash in KOH at different temperatures, molarities, and *W/S* ratios. The highest ratio, $W/S = 40$, was studied previously [1]. There, we showed that three processes in succession control corrosion of the glass phase in six fly ashes: chemical reaction at the surface of spherical particles, diffusion of reactants through a porous layer of reaction products, and diffusion through a dense layer of reaction products. These processes were identified using the modified Jander equation [4, 5].

If a chemical reaction determines the rate of glass dissolution, the contracting volume model (sphere or cube) [6], Eq. 5 can be used:

$$[1 - (1 - \alpha_t)^{1/3}] = K_1 \cdot t \tag{5}$$

where $K_1 = k_1/r_0$ with k being a rate constant, r_0 the initial radius of a sphere, t is time, and α_t as defined in Eq. 2.

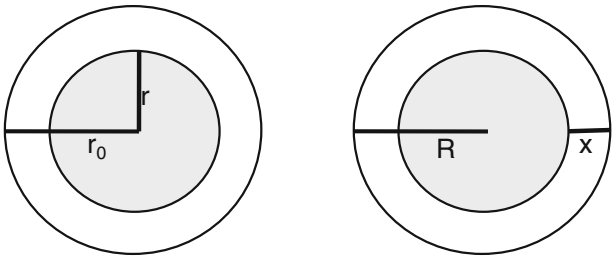

(a) Contracting sphere model **(b)** Diffusion model

Fig. 9 Schematic representation of the contracting sphere model (**a**) and the diffusion model (**b**)

The Jander model is given by Eq. 6. Its derivation from Fick's law can be found in Khawam and Flanagan's work [6].

$$[1 - (1 - \alpha_t)^{1/3}]^2 = K_2 \cdot t \tag{6}$$

where $K_2 = k_2/R^2$ with k_2 being a diffusion constant. A schematic illustrating the models underlying Eqs. 5 and 6 is shown in Fig. 9a, b. In Fig. 9a, r_0 is the initial radius of a sphere and r is the radius after dissolution of a certain fraction of the material. In Fig. 9b, R is the initial radius of a reacting sphere and x designates the thickness of a layer of reaction products on a shrinking core.

Villar-Cociña et al. [7] report that Jander's model is one of the most widely used models to explain pozzolanic reactions. The model is based on the Fick's parabolic law, i.e., it describes the pozzolanic reaction as diffusion controlled. Ginstling and Brounshtein [8] state that the Jander model holds only for small values of x/R (Fig. 9), i.e. for limited reaction progress, because it applies Fick's parabolic law to a sphere, though Fick's law was derived for a plane. Using the correct steady-state solution of Fick's first law for radial diffusion in a sphere [9], Ginstling and Brounshtein [8] developed a model, which is represented by Eq. 7:

$$1 - \frac{2}{3}\alpha_t - (1 - \alpha_t)^{2/3} = k \cdot t \tag{7}$$

where $k = D \cdot C_2 \cdot \mu/(\rho \cdot n)$, D being the diffusion coefficient of the reactant, C_2 the concentration of the reactant at the surface, μ the molecular weight and ρ the density of the reaction product, respectively, and n is the stoichiometric coefficient of the reaction.

If the Ginstling–Brounshtein model is considered the more accurate one, we can calculate the deviation of the Jander model from the Ginstling–Brounshtein model and find that the Jander model overestimates the time it takes to reach a certain α_t value. The deviation (overestimation) increases with increasing α_t and reaches 10% at $\alpha = 0.4$. Since none of our data (Fig. 3) exceeds $\alpha_t \approx 0.4$ on average, use of the Jander model introduces a systematic error of up to 10% into our data interpretation with respect to the Ginstling–Brounshtein model. We will show that most of the data modeled with the Jander model do not exceed $\alpha_t \approx 0.2$, i.e., the associated deviation is ≤5%. The deviation of most of the experimental data at $\alpha_t > 0.2$ ($W/S = 0.35$) exceed by far the predictions of both models. This makes it necessary to find a different model for higher α_t values.

Kondo et al. [5] have modified the Jander equation for broader application by introducing a reaction grade N:

$$\left[1 - (1 - \alpha_t)^{1/3}\right]^N = k \cdot t \tag{8}$$

or in linear form:

$$\ln[1 - (1 - \alpha_t)^{1/3}] = \frac{1}{N}\ln K_N + \frac{1}{N}\ln t \tag{9}$$

where K_N is a rate constant.

Following Kondo et al. [5], Eq. 9 can be used to model consecutive and sometimes overlapping processes. While $N = 1$ and $N = 2$ are represented by Eqs. 5 and 6, Kondo et al. [5] proposed that $N > 2$ in the modified Jander model describes processes controlled by diffusion of reactants through dense layers of reaction products. The modified Jander model applies to spherical particles of uniform size. Most of the fly ash particles are spherical but there is a particle size distribution. This issue will be discussed later.

Shi and Day [10, 11] used Eq. 9 to model reactions of an activator (Na_2SO_4 and $CaCl_2$) in a lime-pozzolan blend. Dabic et al. [12] and Krstulovic and Dabic [13], modeled cement hydration. Cabrera and Rojas [14] modeled hydration of the metakolin–lime–water system.

The W/S ratios 40 and 0.35 are of interest to us. At $W/S = 40$, the mixture of fly ash and 7.5 M KOH solution remained a thin slurry at all times at 75 °C. The results for $W/S = 40$ were discussed previously [1] and are used here in part to compare with findings at $W/S = 0.35$. At this low W/S ratio, we obtained a paste, which solidified within hours, gaining significant strength. After 7 days, the solid geopolymer material appeared and felt dry. Yet, reaction progress increased slowly (Fig. 3).

Using Eq. 9 and data from Figs. 1 and 3, we obtained the results of a kinetic analysis shown in Figs. 10 and 11. Figure 10a shows the data from Fig. 1. The slopes of the curves are the inverse of N. Parallel straight lines were obtained, following the decreasing W/S ratios from left to right. For $W/S = 0.35$ in Fig. 10a, neither Eq. 6 nor 7 can be used to fit our data beyond a certain reaction progress. The same is true for certain reaction progress data shown in Figs. 10b and 11. The higher the temperature the more pronounced is the deviation of model predictions from the data. Using Kondo et al.'s [5] modified Jander model in the form of Eq. 9 changes the picture.

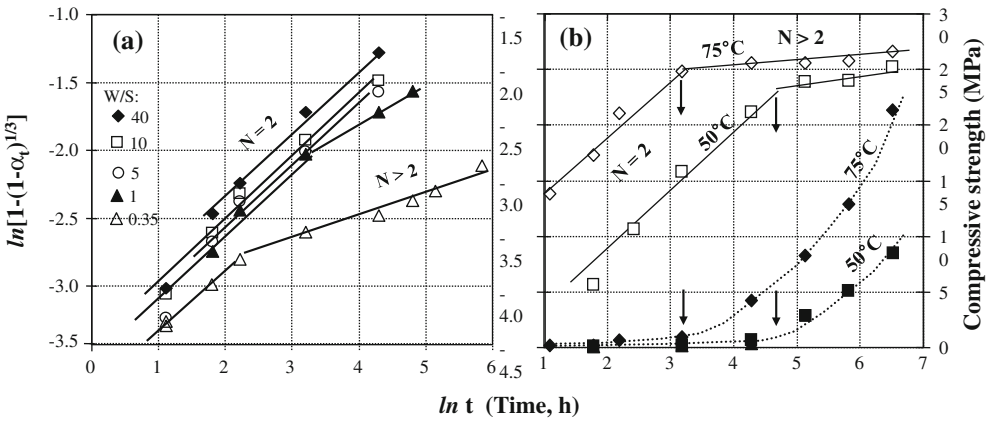

Fig. 10 **a** Effect of water-to-solid ratio on reaction kinetics of fly ash (7.5 M KOH, 75 °C), **b** Reaction kinetics and evolution of compressive strength in 10 M KOH at 50 °C and 75 °C, *W/S* = 0.35 (*arrows* mark increase of compressive strength above 1 MPa). *Open symbols* left scale, *filled symbols* right scale)

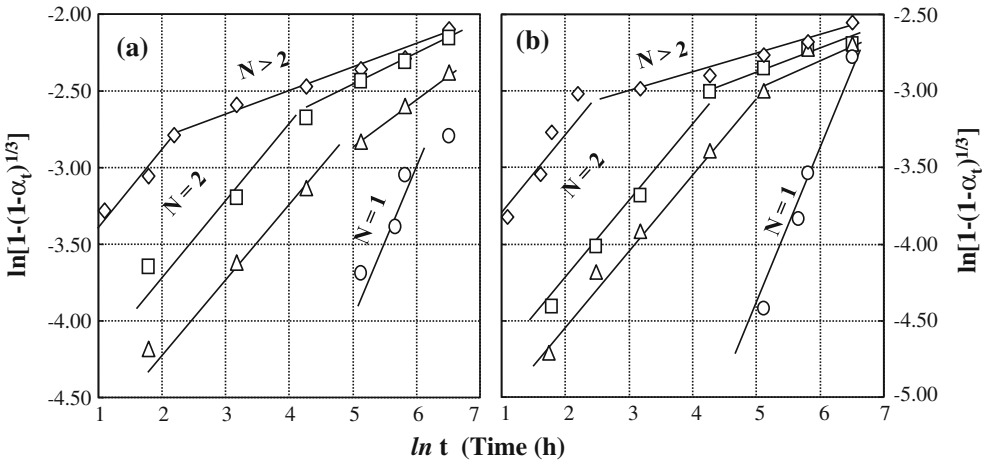

Fig. 11 Kinetic analysis of the process of geopolymerization (**a** 7.5 M, **b** 5 M KOH; both at *W/S* = 0.35). *Open diamond* 75 °C, *open square* 50 °C, *open triangle* 35 °C, *open circle* 22 °C

The kinetic analysis of reaction progress data from Fig. 3 (10 M KOH) is shown in Fig. 10b and for 7.5 M and 5 M KOH in Fig. 11a, b. The compressive strength data in Fig. 10b will be discussed later. Unless mentioned otherwise, all reaction progress data are for $W/S = 0.35$. Straight parallel ($N = 2$) and non-parallel ($N > 2$) lines were obtained, independent of temperature and KOH molarity. Straight lines with $N = 1$ were found only for data measured at 22 °C. The underlying process for $N = 1$ is glass dissolution (Eq. 5, Fig. 11b), relatively the fastest process. The rate is controlled by a first-order chemical reaction. At higher temperatures, the time period of glass dissolution without formation of rate-limiting gel was too short to be measured. The liquid phase saturated quickly with silicon and aluminum species precipitating gel in place, i.e., on the glass surface. Diffusion ($N = 2$) of reactants through this gel layer then controlled further dissolution of the glass (Eq. 6).

SEM pictures (Figs. 7, 8) showed two types of gel, one attached to the glass particles as a relatively thin surface layer, the other completely filling the space between remaining fly ash particles (Fig. 7). The layer of gel surrounding the glass appears brighter in general because it accumulated insoluble hydroxides of heavier elements, i.e., minor constituents from the glass, such as Fe, Ti, Zn, and Ca [1]. This suggests that the interstitial gel contains less high-Z elements relative to Al and Si. The thoroughly and repeatedly washed and then dissolved reaction products (surface and interstitial gel) contained potassium (Fig. 5b), which was not considered contamination from the KOH pore solution. The composition of the surface gel was known from previous work [1]. The surface gel contained

less potassium than found here. Therefore, we assume that the interstitial gel contains most of the potassium.

Under the SEM, the gel surrounding the glass was clearly distinguishable from the interstitial gel after 3 days (Fig. 8) and after 28 days (Fig. 7). Based on our SEM findings, we suggest that hardening of the mixture (fly ash and KOH) begins when the interstitial space between fly ash particles is filled with the darker gel. The kinetics could change at this point from $N = 2$ to $N > 2$ because the remaining liquid phase now resides in meso-pores of the interstitial gel, which are much smaller than the interstices between fly ash particles. Measurements by Skvara et al. [15] show average pore sizes in fly ash geopolymers near 30, 40, and 1,000 nm, depending on preparation conditions. Diffusion in small pores could slow down the transport of reactants toward the glass surface of the pristine glass. OH^- is most likely the rate-limiting species [1].

Fernándes-Jiménes et al. [16] divided the reaction progress into three stages: stage 1 is glass dissolution, stage 2 is an induction period during which metastable gel precipitates (gel 1), which coats the glass particles and incorporates aluminum preferentially. Mechanical strength is still insignificant. In stage 3, the silicon incorporation stage, "gel 1" transforms into "gel 2" by preferentially accommodating silicon species in its structural framework. The transformation renders mechanical strength to the geopolymer. Though our experimental conditions are different, i.e., 10 M KOH, 75 °C and more glass in the fly ash versus 8 M NaOH, 85 °C in [14], our results are in qualitative agreement with Fernándes-Jiménes et al.'s findings. Whether the gel surrounding the glass particles and our "interstitial gel" both undergo structural change remains unresolved at this time.

We find from Figs. 10 and 11 that the kind and the sequence of rate laws are unaffected by changes in *W/S*, KOH concentration, and temperature. What does change, however, is the relative contribution each process makes to the overall reaction progress. We discuss this finding further for $W/S = 0.35$, which is most relevant for the formation of a geopolymer. Using the two consecutive straight lines at 75 °C in Fig. 10b, we calculate that about 70% ($\ln[1 - (1 - \alpha_t)^{1/3}] = -2.7$, $\alpha_t = 0.22$) of the measured reaction progress is controlled by classic Fick diffusion ($N = 2$) and 30% by the slowest transport process ($N > 2$). The contribution of the first-order glass dissolution reaction ($N = 1$) to the total α_t was estimated to be less than 1%. By comparison, for the 22 °C data in Fig. 11a, b, glass dissolution ($N = 1$) controlled the reaction progress up to $\alpha_t \approx 0.22$. We reported earlier [1] that the first-order glass dissolution reaction was accompanied by formation of a surface layer, which contained insoluble minor glass constituents, some silicon, aluminum, and potassium; yet, the layer was obviously not dense or thick enough to control the dissolution rate of the glass by diffusion.

Lowering the KOH concentration from 7.5 to 5 M (Fig. 11b) slowed down all processes and made glass dissolution ($N = 1$) the rate determining process for most of the reaction progress measured at 22 °C. Since nearly the same reaction progress was measured at $N = 1$ as with the other processes at higher temperatures, we continued the experiment for some 300 days, at which time a solid geopolymer had formed with a compressive strength of about 5 MPa (Fig. 4, dark symbols). The reaction progress increased from 0.175 to 0.235, i.e., sufficient gel had formed to provide some mechanical durability.

Increasing the KOH concentration from 7.5 M (Fig. 11a) to 10 M (Fig. 10b) accelerated all processes and extended their ranges of rate-control. At 75 °C, diffusion controlled the reaction progress up to $\alpha_t = 0.35$, i.e., ($\ln[1 - (1 - \alpha_t)^{1/3}] = -2.0$), a range controlled by two processes ($N = 2$ and $N > 2$) in 7.5 M KOH.

At the beginning of fly ash leaching, glass dissolution progresses approximately linearly with time, at all KOH concentrations, as shown in Fig. 3 (22 °C). The solubility of dissolved silicon and aluminum species increases with increasing KOH concentration. Thus, the higher the KOH concentration, the higher is the α_t value at which formation of aluminosilicate oligomers, amorphous polymers, and interstitial gel begins. As soon as enough gel of sufficient density has precipitated on the glass surface, diffusion of presumably hydroxyl groups [1] becomes rate limiting for further dissolution of glass.

While the change from $N = 1$ to $N = 2$ can be explained based on our experimental findings, the point of transition from $N = 2$ to $N > 2$ and the nature of the underlying transport process are less well understood. Figure 5 provides some insight into the transition from one kinetic process to the next, both at high ($W/S = 40$) and low ($W/S = 0.35$) ratios. Experiments with fly ash/KOH mixtures at $W/S = 40$ have been reported by Chu et al. in a previous article [1]. In Fig. 5, we have compiled hitherto unpublished results from previous work together with data from this work. The molar ratio "*R*" of SiO_2/Al_2O_3 in the glass phase of the fly ash is 3.77 (dotted lines in Fig. 5a, b). The earliest chemical analyses of the gels (Fig. 5a, lowest curve and Fig. 5b, upper solid curve) show that both gels are enriched in aluminum, relative to the glass. The respective *R* values are 2.7 (Fig. 5a) and 2.85 (Fig. 5b). With increasing time, the SiO_2 content increases quickly. At $W/S = 40$, the relative increase of silica ends after about 10 h (Fig. 5a). Then, *R* decreases and becomes constant at 2.7, i.e., the gel is still enriched with Al relative to the glass. After 24 h, third datum in Fig. 5a, crystals of zeolite Linde F, $KSiAlO_4 \cdot 1.5H_2O$, were detected by X-ray diffraction, as reported in [1]. Note that *R* values in surface

layers are an average of all solid reaction products of glass leaching (β_t', Eq. 4). In the early stage of leaching, there was little gel (Fig. 2a, $W/S = 40$) and no zeolite had crystallized yet [1]. Most of the glass was simply dissolved (Fig. 2b). Later, the surface layer contained gel with zeolite on top [1]. Therefore, a constant ratio $R \approx 2.7$ means that the surface layer consists of two components, zeolite Linde F ($R = 2$) and amorphous aluminosilicate gel of constant composition with $R_{gel} > 2.7$. However, R_{gel} must be less than 3.77 (glass), because silicon is continuously released into solution (upper curve in Fig. 5a). After 3 days, a layer of crystals surrounded the glass particles, which most likely slowed down the transport of OH^- to the glass surface and thus the reactivity (Eq. 1) of the fly ash. The slow down was marked by the transition from $N = 2$ to $N > 2$. The N values are shown in Fig. 5a.

The situation is different at $W/S = 0.35$ (Fig. 5b). Glass is converted only into gel almost from the very beginning (Fig. 2a). The silicon content of the originally more Al-rich gel increases quickly during the first 24 h and then very slowly to $R = 3.6$ after 28 days. This R value is very close to that of the glass, suggesting that the increase of α_t indicates conversion of glass into gel in situ with little change in composition. Fernándes-Jiménes et al. [16] found a similarly quick enrichment of SiO_2, which they tracked by measuring the diminishing number of $[AlO_4]$ tetrahedra neighboring $[SiO_4]$ tetrahedra. Sagoe-Crentsil and Weng [17] and Weng and Sagoe-Crentsil [18], using meta-kaolin and NaOH, reported that free $Al(OH)_4^-$ groups were not seen in solution, suggesting that the condensation of aluminate and silicate species is fast. The authors report that a second condensation process followed, solely involving silicate species. The findings in [17] and [18] are in qualitative agreement with ours in Fig. 5, in spite of different experimental conditions and materials.

During silica enrichment (Fig. 5b), the K_2O/Al_2O_3 ratio decreases to almost 1:1, yielding a charge-balanced gel. Glass dissolution is diffusion controlled during silica enrichment in the gel. Enrichment slows sharply when the kinetics changes from $N = 2$ to $N > 2$ (Fig. 5b). At this transition point an observation was made, which is shown in Fig. 10b. The transition from $N = 2$ to $N > 2$ marks the point at which the geopolymer paste begins to gain compressive strength. The coincidence is shown for two temperatures and is marked by the arrows in Fig. 10b. The microstructure of the sample (10 M, 75 °C) at the transition point is shown in Fig. 6. The arrows point at areas where gel has formed bridges between particles, which provides already some mechanical durability, in this case about 1 MPa (Fig. 10b). At this point, the pores may well be filled with low-density gel and/or gel-like oligomers, not seen under the SEM. The amount of gel increases relatively fast (Fig. 8), though the increase in α_t is relatively small between 1 day (Fig. 6) and 3 days (Fig. 8). After 28 days (75 °C, last α_t value in Fig. 10), the compressive strength has increased to 22 MPa. The corresponding morphology of the sample is shown in Fig. 7. A continuous gel matrix phase has formed with very little, if any space left between particles.

Another observation is that an increase in temperature decreases the slope of the curves after the transition from $N = 2$ to $N > 2$ at all KOH concentrations. This means that consumption of the remaining glass slows down with increasing temperature. The cause could be that faster restructuring of the gel at higher temperature impedes transport of hydroxyl groups to the glass surface more than at lower temperatures. The common feature is, however, that the suite of processes leads to a common endpoint, i.e., an α_t at which the geopolymer is fully cured. This endpoint appears to be fairly insensitive to the conditions (KOH molarity, temperature) under which it is attained. Calculating this endpoint with confidence, using Eq. 9, would require more data than available at this time for the curves with $N > 2$ in Figs. 10 and 11. Our experiments suggest that a slow diffusion process ($N > 2$) governs the solidification and curing process of a geoplymer. In the absence of this process, i.e., at $N = 1$ or $N = 2$, we did not observe solidification of fly ash.

Next, we address the question whether any crystallization occurred in the course of the fly ash glass leaching process, not seen under the SEM and in X-ray diffraction diagrams. We have conducted X-ray analyses of the vitreous phase and the gel before and after the transition from $N = 2$ to $N > 2$. Small amounts of zeolite, if present, would not be detectable unambiguously because of interference with diffraction peaks from fly ash impurities. To avoid this problem, we synthesized and then reacted the glass phase in with 7.5 M KOH at 75 °C. The synthesis required a slight increase in alkali and alkaline earth content, such that the glass could be melted at about 1,500 °C. The synthetic glass had a slightly higher content of P_2O_5 (0.5 wt%, nominally) than the real fly ash glass (0.1 wt%, measured). Figure 12 shows X-ray diffraction spectra of the pristine glass (curve on the bottom), the glass and gel together (above), a few hours before and after the transition, and then 2 weeks later. To detect any crystalline phases, the samples had to be measured in step-scan mode over several hours. A small amount of magnetite (Fe_3O_4) crystallized from the pristine glass, which reacted at high pH, yielding ferrihydrite ($Fe_5O_7(OH)\cdot 4H_2O$) and later vivianite ($Fe_3(PO_4)_2\cdot 8H_2O$). Though not marked in the spectra, the samples measured shortly after and 2 weeks after the transition still contain magnetite and ferrihydrite. No commonly known zeolite matched the unmarked peaks. The crystalline phase yielding the diffraction peaks is still unknown. Overall, the hardening geopolymer is essentially

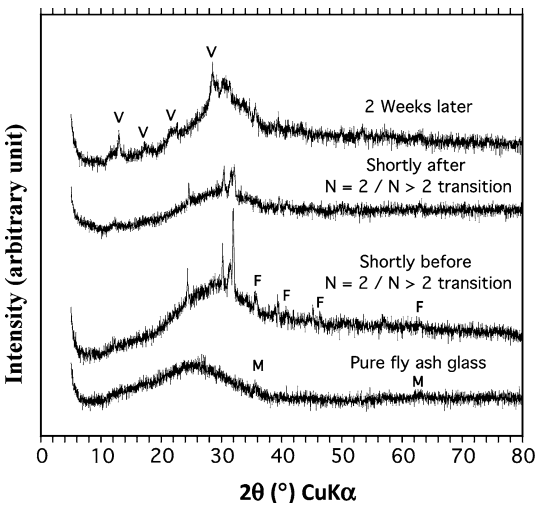

Fig. 12 X-ray diffraction patterns of synthesized pristine and reacted glass before and after the transition from $N = 2$ to $N > 2$ (7.5 M KOH, 75 °C, $W/S = 0.35$); *M* magnetite

X-ray amorphous. It is the matter of further research to find out, to what extent the changes in shape and intensity of the hump at $2\Theta \approx 30°$ can be related to the change of the slopes N. More detailed characterization of inorganic polymer gel compositions have become a powerful tool to understand mechanisms of gel formation and thus of the hardening process [19–21].

Recently, Lloyd et al. [20, 21] published microscopy and microanalysis results of inorganic polymer cement (IPC). We would like to address some differences between findings in [21] and here. We refer specifically to gel formation in hydroxide-activated fly ash [21] and to experiments with the most similar conditions (hydroxide molarity, temperature, and *W/S* ratio). However, we used KOH, whereas Lloyd et al. [21] used NaOH. As far as formation of surface layers on the dissolving glass particles is concerned the findings are the same. However, with increasing reaction progress, Lloyd et al. show that surface layers, containing zeolite and gel, grow together eventually, producing a solid with large interstitial space, in contrast to pores in our samples, which are filled with a second gel and no zeolite anywhere. Though zeolites form in both systems [1, 21], one may assume that nucleation is different for sodium and potassium zeolites, which would explain in our case that a gel, rather than crystals, precipitated from the supersaturated solution in the interstices.

Finally, we discuss the effect of shape and size of the reacting glass particles. Most of the fly ash glass particles are spherical. The glass forms at high temperature and surface tension shapes the particles into spheres. However, the glass particles are not uniform in size. Typically, particle size ranges from about 10–80 μm in diameter [1]. Frequently, about 30% of the particles in a fly ash are >45 μm. Since the particle radius is contained in all models (Eqs. 5–8), samples with varying particle sizes will have variable reaction rate constants and this leads to a shift of α_t–time curves. These effects have been described, e.g., by Koga and Criado [22, 23]. Smaller particles leach faster than large particles. The contribution of smaller and larger particles to a given α_t value depends on the mass fraction in size class of each particles. The objective of this work was to identify kinetic processes governing the formation of a simple fly ash geopolymer. The facts that fly ash glass particles have a size distribution make it impossible to calculate accurate reaction rate constants, diffusion coefficients, etc. However, the experimental data show that an effect from non-uniform particle size on our α–time curves is not significant enough to mask the underlying kinetic processes and their succession.

If all glass particles were of the same size, one would see the shortest possible ranges of transitions ($\Delta\alpha$) between two consecutive processes (slopes of the curves in Figs. 10, 11). One would expect a mixture of glass particles of different sizes to widen these ranges. Figure 6 shows small (s), medium-size (m), and large (l) particles. If different processes were in progress in each of these particles, one would expect the transition from $N = 2$ to $N > 2$ in Figs. 10 and 11 to be continuous. Unfortunately, the limited amount of data does not allow us to judge whether the transition is as sharp as it appears to be. A study with a narrow sieve fraction of synthetic fly ash glass particles is in progress to evaluate the effect of a particle size distribution on the results and to calculate rate constants and their temperature dependence. In any case, the measurements show that the three consecutive processes are controlling glass dissolution as a function of reaction progress and that Kondo et al.'s modified Jander model [5], though in part still empirical, describes them well.

Conclusions

We find that three consecutive kinetic processes control reaction progress of fly ash during geopolymerization: (1) a first-order surface reaction between the glass phase in the fly ash and the alkali hydroxide solution, (2) classical Fick diffusion through a surface layer, and (3) diffusive transport through a more complex gel structure (interstitial gel). This sequence is independent of *W/S* (0.35–40), temperature (22–75 °C), and KOH concentration (5–10 M). However, the relative contribution of each process to the overall reaction progress changes with the experimental conditions. After the transition from the second to the third process, interstitial gel fills the space between fly ash particles quickly, i.e. a matrix phase forms, embedding glass particles covered with their own gel layer. Most of

the residual fluid should now be contained in the pores of the matrix phase. The pores could constitute an additional diffusion barrier, causing the change of the kinetic process from $N = 2$ to $N > 2$. A solid fly ash geopolymer can form and develop mechanical strength, only if and when the third process ($N > 2$) is rate controlling.

Acknowledgements The authors are grateful for financial support of this project from the Vitreous State Laboratory (VSL) of the Catholic University of America (CUA). Chen Chen thanks the Chinese Overseas Fellowship Commission for financial support of his visit to VSL/CUA. The authors thank Drs. Hong Zhao, Andrew Buechele, and David McKeown (all VSL) for discussions and experimental support.

References

1. Chen C, Gong WL, Lutze W, Pegg IL, Zhai JP (2010) J Mater Sci. doi:10.1007/s10853-010-4997-z
2. Provis JL, Duxon P, van Deventer JSJ, Lukey GC (2005) Chem Eng Res Des 83:853
3. Provis JL, van Deventer JSJ (2007) Chem Eng Sci 62:2309
4. Jander G (1927) Zeitschrift Anorg Allgem Chem 163:1
5. Kondo R, Lee K, Diamon M (1976) J Ceram Soc (Jpn) 84:573
6. Khawam A, Flanagan DR (2006) J Phys Chem 110:17315
7. Villar-Cociña E, Frías M, Valencia-Morales E, Sánches de Rojas MI (2010) Adv Cem Res 18:17
8. Ginstling AM, Brounshtein BI (1950) J Appl Chem USSR 23:1327
9. Crank J (1975) The mathematics of diffusion, chap 6, 2nd edn. Clarendon Press, Oxford, p 89
10. Shi CJ, Day RL (2000) Cem Concr Res 30:51
11. Shi CJ, Day RL (2000) Cem Concr Res 30:607
12. Dabic P, Krstulovic R, Rusic D (2000) Cem Concr Res 30:1017
13. Krstulovic R, Dabic P (2000) Cem Concr Res 30:693
14. Cabrera J, Rojas MF (2001) Cem Concr Res 31:177
15. Skavara F, Kopecky L, Nemecek J, Bittnar Z (2006) Ceram Silikaty 50(4):208
16. Fernández-Jiménez A, Palomo A, Sobrados I, Sans J (2006) Micropor Mesopor Mater 91:111
17. Sagoe-Crentsil K, Weng L (2007) J Mater Sci 42:3007. doi:10.1007/s10853-006-0818-9
18. Weng L, Sagoe-Crentsil K (2007) J Mater Sci 42:2997. doi:10.1007/s10853-006-0820-2
19. Zaharaki D, Komnitsas K, Perdikatsis V (2010) J Mater Sci 45:2715. doi:10.1007/s10853-010-4257-2
20. Lloyd R, Provis JL, van Deventer JSJ (2009) J Mater Sci 44:608. doi:10.1007/s10853-008-3077-0
21. Lloyd R, Provis JL, van Deventer JSJ (2009) J Mater Sci 44:620. doi:10.1007/s10853-008-3078-z
22. Koga N, Criadi JM (1998) J Am Ceram Soc 81:2901
23. Koga N, Criadi JM (1997) J Therm Anal 49:1477